Journal of The
Electrochemical Society

Highly Graphitic, Mesoporous Carbon Materials as Electrocatalysts for Vanadium Redox Reactions in All-Vanadium Redox-Flow Batteries

To cite this article: Stefan Rümmler *et al* 2018 *J. Electrochem. Soc.* **165** A2510

Highly Graphitic, Mesoporous Carbon Materials as Electrocatalysts for Vanadium Redox Reactions in All-Vanadium Redox-Flow Batteries

Stefan Rümmler,[1] Matthias Steimecke,[1] Sabine Schimpf,[1] Mark Hartmann,[1] Stefan Förster,[2] and Michael Bron [1,z]

[1]*Martin-Luther-Universität Halle-Wittenberg, Naturwissenschaftliche Fakultät II, Institut für Chemie, Technische Chemie I, D-06120 Halle, Germany*
[2]*Martin-Luther-Universität Halle-Wittenberg, Naturwissenschaftliche Fakultät II, Institut für Physik, FG Oberflächen- und Grenzflächenphysik, D-06120 Halle, Germany*

Two new commercially available mesoporous graphitic carbon materials were oxygen-functionalized with 0.2 M potassium permanganate solution, 10 M nitric acid and a mixture of water, nitric and sulfuric acid in a ratio of 1:2:1, respectively. Heat treatment of the oxidized samples in the presence of urea as a nitrogen precursor at 800°C yielded nitrogen-containing surface functional groups. Functionalized samples are compared to the pristine materials with respect to structure and morphology using TGA, Raman spectroscopy, TEM and XPS. The degree of oxygen functionalization depends on the oxidation agent and is different for both materials. There is a weak correlation between the amount of oxygen functional groups and the amount of nitrogen implemented during urea treatment, with thermally more stable C-O oxygen groups leading to enhanced nitrogen incorporation. The samples show a considerable structural inhomogeneity as observed from Raman spectroscopy in a mapping mode collecting 300 spectra. Electrocatalytic activity toward the VO^{2+}/VO_2^+ redox pair was determined by CV. The electrocatalytic activity of the materials is significantly increased after functionalization, however, surprisingly independent from the degree of functionalization. On the other hand, carbon structural properties seem to have a significant impact on activity.
 [DOI: 10.1149/2.1251810jes]

Manuscript submitted May 17, 2018; revised manuscript received July 13, 2018. Published August 16, 2018.

The increasing worldwide energy consumption accompanied by a growing share of fluctuating renewable energy calls for efficient means for energy conversion and storage. Research toward commercially viable large-scale, cheap and stable battery systems is of major importance to face this challenge. The all-vanadium redox flow battery (VRFB) represents one of the currently intensely investigated promising energy storage systems. In a VRFB, intermittent renewable energy from solar and wind power is converted into chemical energy using redox active chemicals dissolved in electrolyte solutions.[1–10] The reactive species are the VO^{2+}/VO_2^+ and V^{3+}/V^{2+} redox couples, which typically are converted at carbon-based electrodes made of graphite, carbon nanotubes, carbon fibers or carbon non-woven[11–18] according to the following equations:

Positive half-cell reaction:

$$V O^{2+} + 3\ H_2O \xrightarrow{charge} V O_2^+ + 2\ H_3O^+ + e^- \quad [1]$$

Negative half-cell reaction:

$$V^{3+} + e^- \xrightarrow{charge} V^{2+} \quad [2]$$

Cell voltage (pH = 0):

$$E = \varphi_{neg} - \varphi_{pos} = -0.26\ V - 1.00\ V = -1.26\ V \quad [3]$$

Equations 1 and 2 describe the charging process, while during discharging the reverse reactions will operate. The development of the VRFB started with the seminal work of Skyllas-Kazacos and coworkers, who developed an entire battery system.[1,2] Such redox flow battery systems consists of two tanks for both anolyte and catholyte, two pumps for constant electrolyte flow and one or more electrochemical cells. Typically several electrochemical cells are arranged in series as so-called stacks. One of the big advantages of VRFB is that the power output may be controlled independently by the size of the stack (i.e. electrode area, number of individual cells). Each of the cells are separated by a membrane into two half cells. The membrane could be proton exchanging (e.g. Nafion) or anion exchanging, however in industrial applications only cation exchange membranes are used.[8,19,20] The amount of energy stored in a VRFB is only limited by the size of its tanks and the concentration of vanadium species in solution and is independent of the power output.[20] The kinetics of both electrochemical oxidation and reduction of vanadium species on carbon electrodes and the resulting power density of the battery are, among others, determined by surface structure, functional surface groups and orientation of edges and planes as demonstrated for different carbon materials.[20–22] For efficient and profitable long-term application, current research is not only focusing on activity, but also on stability of the electrodes, which is typically claimed to be higher for graphitic than for amorphous materials.

This paper investigates Porocarb (Heraeus), a new highly graphitic material with a large amount of tunable meso- and macropores, toward its performance as electrocatalytically active material for vanadium redox reactions. Porocarb materials were recently introduced successfully as conductivity additive in Li-ion batteries due to their high degree of graphitization and porosity.[23,24] Similarly, the selection of this material for investigations toward VRFB reactions is based on the reported huge influence of the degree of graphitization on conductivity and reactivity concerning the vanadium species conversion.[12,25,26] Furthermore, the tunable porosity may later on help to optimize electrodes toward mass transport properties.

It is quite common to functionalize carbon surfaces using oxidation agents like nitric acid or potassium permanganate or by performing a heat-treatment in the presence of nitrogen-containing precursors with the aim of changing the electrocatalytic behavior (via modified electronic structure or active sites) or enhancing the hydrophilicity by introducing defects or oxygen and/or nitrogen functional groups into the graphitic surface.[27–32] However, the effect of functional surface groups on vanadium redox reactions is discussed controversially. Most publications report activity enhancements of functionalized carbon materials.[11,12,33,34] On the other hand Friedl et al. reported that even strong functionalization has no beneficial effect on the kinetics of the VO^{2+}/VO_2^+ redox reaction at CNTs.[35] Similarly, it was recently shown that surface oxygen functional groups improve the catalytic activity of multi-walled CNTs toward vanadium redox reactions due to improved wetting up to about 3% of surface oxygen, while higher oxygen surface concentrations did not alter the properties of the multi-walled CNTs significantly.[36] On the other hand, the influence of nitrogen functional groups was not investigated in such detail

[z]E-mail: michael.bron@chemie.uni-halle.de

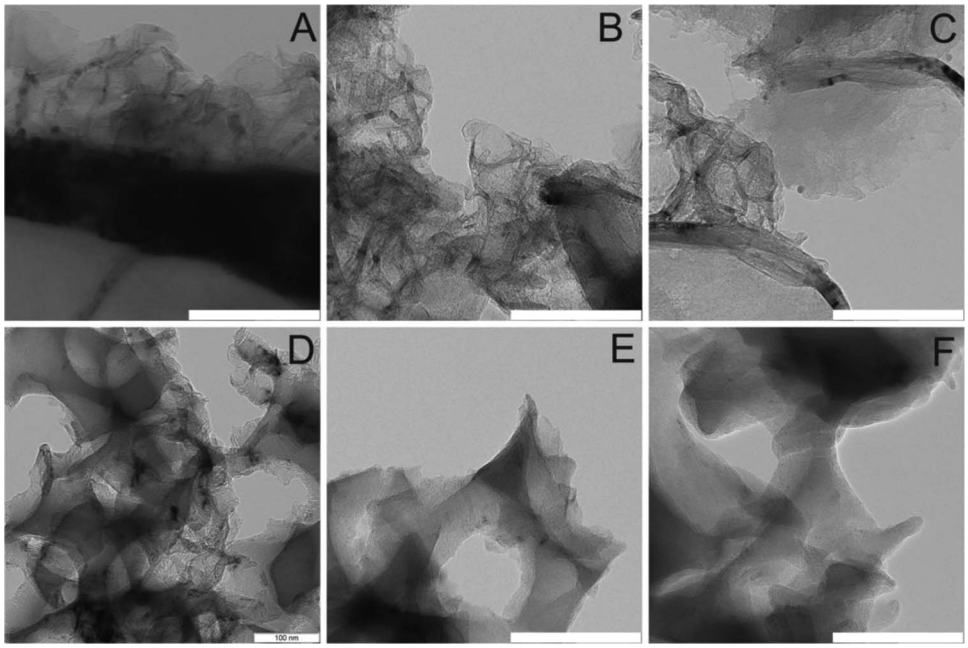

Figure 1. TEM images of HG3 (a), HG3_NASA (b), HG3_NASA_U (c), LG2N (d), LG2N_NASA (e) and LG2N_NASA_U (f), scale bars represent 100 nm.

as for oxygen groups. However, some studies point out that nitrogen introduced into carbon materials enhances the electrocatalytic activity toward the vanadium redox reactions.[37–39] Thus, nitrogen functionalized Porocarb materials are an additional subject of investigation in this study.

The discrepancy in literature regarding the influence of oxygen functional groups points to a lack of understanding of the real kinetics of vanadium species conversion at carbon surfaces including adsorption, charge transfer and desorption. The comparison of results obtained on different carbon materials is complicated due to the fact that structural properties (e.g. ratio of edges and basal planes, carbon hybridization) as well as electronic (i.e. density of state (DOS)) properties of the surface depend on the carbon modification. Thus, not only the surface functional groups but also the electrocatalytically active carbon species itself must be considered.[27,33]

In this paper, two different commercial porous graphitic carbons (Porocarb), as received and surface functionalized, are compared toward their electrocatalytic properties, in particular for the VO^{2+}/VO_2^+ redox pair, which has been claimed to be the kinetically more inhibited reaction in an all-vanadium redox flow battery (VRFB).[40,41] The materials are characterized toward structure and morphology to unravel factors influencing the catalytic activity. For this purpose, X-ray photoelectron spectroscopy (XPS) was used to analyze the chemical composition of the surface, thermogravimetric analysis (TGA) was employed to determine the amount of instable oxygen containing functional groups and transmission electron microscopy (TEM) was performed to obtain morphological information. Furthermore, Raman spectroscopy was carried out to unravel structure and structural changes implemented into the carbon lattice by functionalization, while cyclic voltammetry (CV) served as characterization technique to estimate electrocatalytic activity. Often, rate constants are calculated based on single CV measurements and correlated for example with results from Raman or XPS investigations. As demonstrated in this paper, depending on the carbon material single CV or Raman measurements might be insufficient. In contrast, this study focuses on a qualitative characterization using solid statistics.

Experimental

Porocarb functionalization.—For oxygen functionalization two Porocarb modifications (Porocarb HG3, Porocarb LG2N, Heraeus Deutschland GmbH & Co. KG, Hanau) were treated in solutions of various oxidation agents. 500 mg of the carbon material were suspended in 100 ml of either 10 M nitric acid ("NA", Carl Roth, 65%) or 0.2 M potassium permanganate solution ("PP", Carl Roth, 99%) or a mixture of water, sulfuric acid (Carl Roth, 98%) and nitric acid in a ratio of 1:2:1 ("NASA"). The suspensions were dispersed with the help of an ultrasonic bath for 30 min and afterwards heated up in a microwave oven ("Start", MLS GmbH, Leutkirch) with 800 W, allowing the solvents to boil (∼100°C) under reflux conditions for 1 h (note that nitrous fumes evolve during this procedure). Microwave heating was used instead of a conventional oil bath since it was shown that under microwave conditions functionalization is much more efficient.[32] Then, the acid treated samples were washed several times with distilled water until pH = 7 was reached, using a centrifuge 5804 (Eppendorf) to separate solvent and Porocarb material. Afterwards, the samples were dried in an oven at 100°C in air for 16 h. Permanganate treated samples were additionally suspended in concentrated hydrochloric acid to remove residual impurities of manganese oxides. This procedure was repeated several times to obtain a manganese free carbon surface as verified by XPS.

Furthermore, pristine Porocarb as well as all oxidized samples were treated with urea ("U") in a high temperature process. 80 mg of the respective carbon sample were mixed with 1.2 g urea (Carl Roth, 99.5%), 5 mL distilled water and 15 mL ethanol (Th. Geyer, 99.9%) and the suspensions were dried under stirring at room temperature for two days. The solid mixtures were put onto a quartz boat introduced into a quartz tube located in a horizontal tube furnace. Subsequently, the system was flushed with argon (Air Liquide, 99.999%), heated up to 800°C with 10 K min^{-1} and kept at this temperature for 2 h under constant argon flow. After cooling, the samples were weighted to determine the mass losses. Treatments, corresponding sample names and respective mass losses are given in Table I.

Transmission electron microscopy.—Transmission electron microscopy (TEM) was performed with a LEO 912 OMEGA microscope working at 120 kV. A mixture of several μg of the respective sample and 0.75 ml of ethanol was treated in an ultrasonic bath for 3 h. Subsequently, a 3.05 mm copper grid (300 mesh) was drop-coated using a pipette tip containing few μL of the resulting suspension.

Table I. Sample designations, treatment procedures and resulting mass losses. Last two columns: samples after additional urea treatment (see experimental).

treatment	sample name	mass loss/%	sample name	mass loss/%
-	HG3	-	HG3_U	5.6
10 M HNO_3, 100°C	HG3_NA	1.1	HG3_NA_U	12.3
0.2 M $KMnO_4$, 100°C	HG3_PP	8.4	HG3_PP_U	12.1
H_2O H_2SO_4 HNO_3 1:2:1, 100°C	HG3_NASA	3.5	HG3_NASA_U	12.7
-	LG2N	-	LG2N_U	9.3
10 M HNO_3, 100°C	LG2N_NA	3.6	LG2N_NA_U	8.1
0.2 M $KMnO_4$, 100°C	LG2N_PP	6.9	LG2N_PP_U	60.6
H_2O H_2SO_4 HNO_3 1:2:1, 100°C	LG2N_NASA	2.0	LG2N_NASA_U	12.8

X-ray photoelectron spectroscopy.—Surface characterization was carried out with the help of X-ray photoelectron spectroscopy (XPS). A DAR 400 X-ray source using Al K_α radiation (1486.6 eV) and an EA 125X hemispherical energy analyzer (Omicron) were used. Overview scans were performed with 100 eV pass energy and detail scans of the O*1s* and N*1s* core level regions with 30 eV. Data were fitted and analyzed using the CasaXPS software yielding element ratios and binding characteristics of oxygen and nitrogen.

Thermogravimetric analysis.—Thermogravimetric analyses (TGA) were performed with a Netzsch STA449 F1 Jupiter thermobalance. An alumina crucible was filled with 10 mg of the respective carbon sample and placed in the oven of the TGA instrument, which was evacuated and flushed with argon (Air Liquide, 99.999%) several times to remove residual gas impurities. The samples were investigated under argon flow (50 ml min^{-1}) as well as under argon/oxygen (Air Liquide, 99.998%) flow (3:1 ratio, 50 ml min^{-1}) from room temperature to 1000°C with a heating rate of 10 K min^{-1}.

Raman spectroscopy.—For Raman spectroscopy an InVia Raman spectrometer (Renishaw) with a microscope, a Cobolt CW DPSS Laser (532 nm excitation wavelength), a 1800 l mm^{-1} grating and a CCD camera were used. A small amount of the carbon material was placed on a glass slide. Spectra were recorded with a x100 objective creating a laser spot size of ~1 μm on the sample surface. Additionally, Raman mappings were performed with the help of an XY stage (Prior, 100 nm resolution) in 500 nm steps scanning areas of 10 × 10 μm of the respective sample to evaluate homogeneity.

Electrolyte solution.—A 0.01 M vanadium (IV) solution in a 0.5 M hydrogen sulfate/sulfate buffer (1:1 molar ratio, pH = 2) was used for electrochemical analysis. The lower concentrations compared to industrial solutions allow for a more accurate distinction between the individual catalysts. It is similarly important to minimize conductivity issues.[42] The solution was prepared by dissolving $VOSO_4 \cdot xH_2O$ (Sigma-Aldrich, 99.99%), $KHSO_4$ (Carl Roth, 99%) and K_2SO_4 (VEB Jenapharm) in MilliQ water (< 0.055 μS cm^{-1}).

Electrochemical characterization.—To evaluate the electrocatalytic activity of the Porocarb materials, cyclic voltammetry (CV) of thin film electrodes was performed. For electrode preparation, inks of Porocarb were prepared by suspending 20 mg of Porocarb in 2 mL acetone (Carl Roth, 99.5%) and 5 μl of Nafion 117 solution (Sigma-Aldrich, 5 wt% in lower aliphatic alcohols). These suspensions were treated in an ultrasonic bath (Sonorex) for 5 h, which was thermostated to 20°C. A GC (glassy carbon) electrode (4 mm in diameter, embedded in a PTFE cylinder) was cleaned with alumina oxide polishing paste (1.0 and 0.3 μm) and with distilled water on a polishing cloth before each measurement. After ultrasonic treatment of the suspension, 5 μl of the ink was pipetted onto the cleaned GC tip electrode giving a loading of 50 μg and resulting in a homogeneous film. Afterwards, cyclic voltammograms were recorded in N_2 purged 0.01 M $VOSO_4$ buffered solution (see above) in a three-electrode one compartment glass cell in the potential range between 0.0 and 1.0 V vs. $Ag|AgCl|KCl_{sat}$ at a scan rate of 50 mV s^{-1}. The glassy carbon (GC) electrode covered with the sample served as working electrode (WE), an $Ag|AgCl|KCl_{sat}$ electrode as reference electrode (RE) and a Pt mesh as counter electrode (CE). Cyclic voltammograms were recorded with a Gamry potentiostat PGI4 controlled by the Gamry Framework 2.67 software. Five cycles were recorded. In case all cycles showed constant behavior, the fifth cycle is represented and discussed, otherwise the deviating cycles will be discussed separately.

Results and Discussion

Comparison of pristine porocarb modifications.—Porocarb materials are a class of highly graphitic, porous synthetic carbons manufactured by Heraeus, which are offered with different fundamental physical properties. According to the sample data sheets, the tap density of Porocarb LG2N is 280 kg m^{-3} and thus twice the tap density of Porocarb HG3 Fine Grain (150 kg m^{-3}), however, the surface area of the latter is 55 m^2 g^{-1} and thus three times higher than for LG2N with 17 m^2 g^{-1}. The particle sizes are between 3 and 4 μm and are the same for both modifications. The pore volume amounts to 0.9 cm^3 g^{-1} for LG2N with broad and homogeneous diameter distribution from 40 nm up to 8 μm. HG3 has a 2.35 cm^3 g^{-1} cumulative pore volume with a less homogeneous diameter distribution from 20 nm to 800 nm.

Morphology determination by TEM.—Possible differences in morphology of both Porocarb modifications as well as changes introduced by functionalization were analyzed by TEM. Figures 1a–1c show images of pristine HG3 as well as the oxidized and the urea treated samples, Figures 1d–1f show similar images of the LG2N equivalents. Graphene- or graphite-like layers seem to be visible in all structures, with the less dense HG3 structure appearing more open and less compact compared to the more solid morphology of LG2N, which is consistent with the difference in tap density between these two modifications. A certain porosity is visible in particular in the case of LG2N. However, it also seems to be present in HG3. Besides the graphitic structures, also less ordered or amorphous material is visible in the pristine samples. Clear morphological changes are introduced by functionalization. The edges of LG2N are smoothened, the amorphous material disappears partially after oxidation and completely after urea treatment. On the other hand, this smoothing is not observed for the HG3 modification but the surface seems to become rougher, which is however difficult to judge from TEM measurements. From TEM it is thus very obvious that HG3 and LG2N not only differ in their macroscopic properties, like surface area and density, but also in their microstructure. The changes introduced into this microstructure by functionalization are different for both materials.

X-ray photoelectron spectroscopy.—The atomic composition in the near surface region as well as the nature of surface functional groups of the various samples was analyzed by XPS. Examples of the obtained photoelectron spectra are shown in Figure 2. Figure 2a shows a typical overview scan which reveals the presence of O, N and C only. Additionally, detail scans of the oxygen and nitrogen regions are given in Figures 2b and 2c. The atomic compositions of all samples are summarized in Table II for surface oxygen and in Table III for surface nitrogen, respectively.

Table II. Overall surface oxygen content obtained from XPS and distribution among binding energies respectively bonding situations of functional groups of oxidized Porocarb samples. All values in [at%].

sample name	O 1s	C–O 532.7–533.8 eV	C=O 531.4–532.5 eV
HG3	2.0	2.0	0.0
HG3_NA	4.0	3.4	0.6
HG3_PP	4.5	3.2	1.3
HG3_NASA	6.0	5.2	0.8
LG2N	3.0	2.4	0.6
LG2N_NA	6.3	3.5	2.8
LG2N_PP	8.8	7.5	1.3
LG2N_NASA	11.0	5.5	5.5

From Table II it is obvious that all applied treatments lead to higher concentrations of oxygen at the surface. However, both modifications react differently to each individual treatment. In general, LG2N seems to incorporate a much higher amount of oxygen compared to HG3, with NASA-treated HG3 having 6% and NASA-treated LG2N having 11% of surface oxygen. Note that already the pristine samples contain surface oxygen in the amounts of 2% (HG3) or 3% (LG2N). However, the different treatments also lead to a different distribution in functional groups. Binding energies in the range of 533.2 ± 0.3 eV represent hydroxyl and ether groups as well as single bonded oxygen in ester and carboxyl groups. Oxygen-carbon double bonds show binding energies of 531.6 ± 0.3 eV, i.e. functional groups such as ketones or quinone structures and also carbonyl oxygen in ester and carboxyl groups.[28] Obviously, the C-O/C=O ratio is relatively higher for the NA or NASA treated HG3 samples (low amounts of C=O), while the same LG2N samples show a relatively lower ratio (high amounts of C=O). On the other hand, the PP treated LG2N sample shows a higher C-O/C=O ratio compared to the HG3 one, attributed to the high amount of C-O-groups in the former sample. Therefore, it can be assumed that structural differences between HG3 and LG2N influence the reaction behavior and the formation of functional groups.

Nitrogen incorporation by urea treatment leads to a variety of surface nitrogen groups as displayed in Figure 2c and Table III. However, two contributions dominate the N1s region, attributed to terminal end groups and in particular amine structures with binding energies of about 399.2 ± 0.4 eV as well as pyrrole structures at 400.1 ± 0.3 eV.[43] This indicates, that the majority of the introduced nitrogen is linked by one or two single bonds to the carbon network. Although it seems that a certain amount of surface oxygen, probably as reactive sites, is necessary to promote incorporation of nitrogen into the carbon surface,[44] there is only a weak correlation between the total amount of surface oxygen before urea treatment and that of implemented nitrogen, and O_{before}/N-values range from 1.8 for LG2N_PP_U to 5.2 for LG2N_NASA_U. This indicates, that additional structural factors of the carbon substrate are of importance for the incorporation of nitrogen. This is corroborated by the fact that after urea treatment there is still a significant oxygen concentration present in the samples. However, this oxygen could also result from post urea-treatment during handling in air at ambient temperature. The ability to implement nitrogen is obviously higher for LG2N than that for HG3. It also seems that there is a weak correlation between the amount of C-O-bonds and the total nitrogen, and the C-O_{before}/N ratio is 2.6–3.5 for HG3

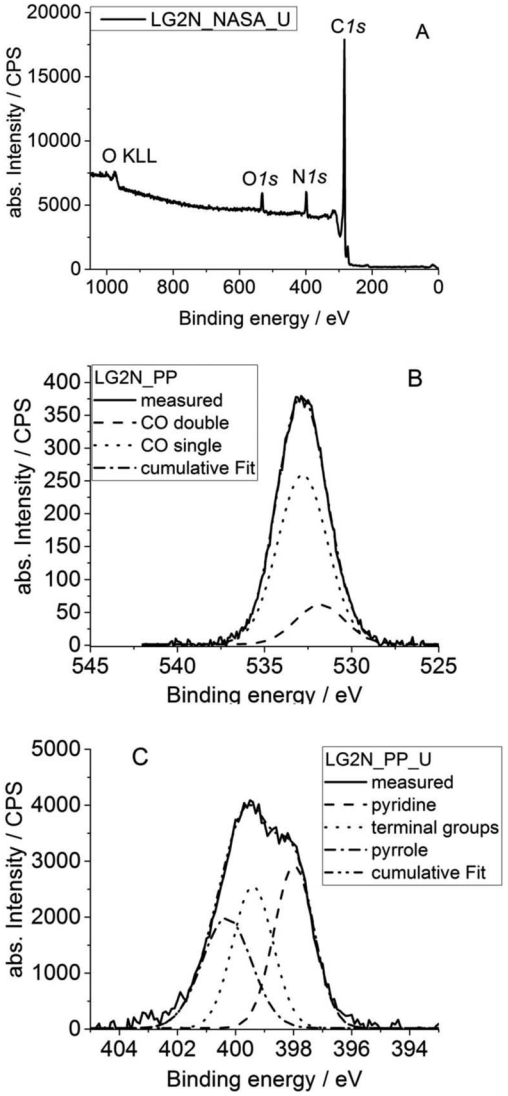

Figure 2. XPS overview scan of the functionalized LG2N sample with O 1s at 532 eV, N 1s at 399 eV and C 1s at 284 eV (a), O 1s detail scan of LG2N_PP with two peak fits for carbon oxygen single and double bond (b) and N 1s detail scan of LG2N_PP_U with three peak fits for pyridine, terminal and pyrrole groups (c).

Table III. Overall surface nitrogen content of urea-treated samples and distribution among the different species integrated into the carbon surface. All values in [at%].

sample name	N 1s	$NH_{x\ adsorbed}$ 397.0 ± 0.3 eV	$N_{pyridine}$ 398.1 ± 0.3 eV	$N_{terminal}$ 399.2 ± 0.4 eV	$N_{pyrrole}$ 400.0 ± 0.3 eV	$N_{quaternary}$ 401.5 ± 0.3 eV
HG3_U	-	-	-	-	-	-
HG3_NA_U	1.3	0.1	-	0.9	0.1	0.2
HG3_PP_U	0.9	-	0.1	0.2	0.4	0.2
HG3_NASA_U	1.6	-	-	1.2	0.3	0.1
LG2N_U	1.2	-	-	1.0	0.1	0.1
LG2N_NA_U	3.2	0.2	-	1.4	1.4	0.2
LG2N_PP_U	4.8	-	1.8	1.5	1.5	-
LG2N_NASA_U	2.1	-	0.3	0.7	0.9	0.2

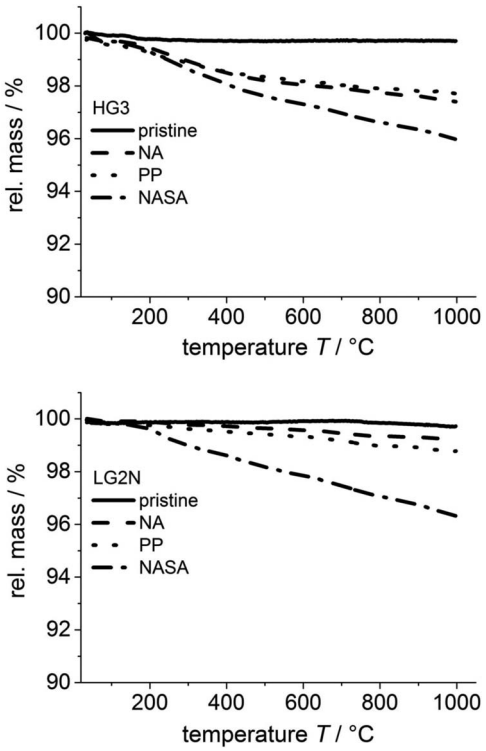

Figure 3. Decomposition curves up to 1000°C in Ar atmosphere of oxidized HG3 (upper) and LG2N (lower) samples.

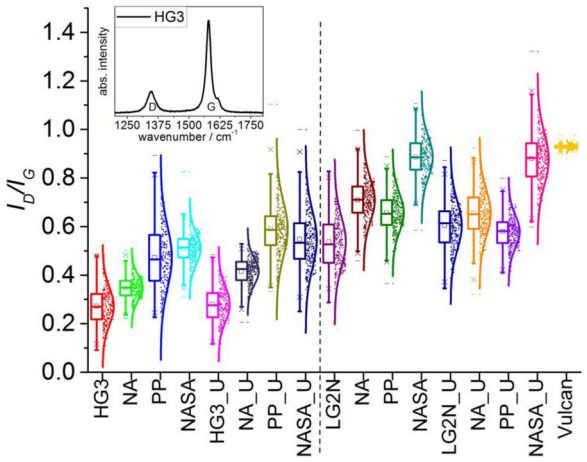

Figure 4. Box plot diagram of the I_D/I_G values from Raman mappings carried out for all samples containing 250–300 individual spectra per sample. Inset: Raman spectrum of pristine HG3 measured with 532 nm excitation wavelength.

and 1.1–2.6 for LG2N, with the untreated HG3 sample as an exception (see supporting information, Figure S1). LG2N_PP_U possesses the highest amount of surface nitrogen up to 4.8 at% including a third nitrogen species identified as pyridinic N at 398.1 ± 0.3 eV.[43] Furthermore, all three nitrogen species are present in equal amounts, while acid treated LG2N shows only pyrrole and terminal nitrogen species after urea heat-treatment.

Thermogravimetric analysis.—Thermogravimetric analysis in argon atmosphere was employed in conjunction with the XPS results to obtain additional information about the chemical composition and stability of the carbon surfaces. Oxygen containing functional groups such as hydroxyl and carboxyl species bound to carbon networks decompose in inert gas atmosphere in the temperature range from 150 to 450°C according to the following chemical equations:[45]

$$RCOH \xrightarrow{\Delta T} RH + CO \quad [4]$$

$$2\,RCOH \xrightarrow{\Delta T} ROR + H_2O \quad [5]$$

$$RCOOH \xrightarrow{\Delta T} RH + CO_2 \quad [6]$$

At higher temperatures the decomposition of anhydrides and lactones may be observed.[28] Thus, the mass loss of the oxidized samples during TGA in argon atmosphere should correlate with the amount of these functional groups. Figure 3 displays the respective decomposition curves. Generally, mass losses are between about 0.5 wt% for the pristine and 4 wt% for the NASA-treated samples, and as expected the mass loss depends on the oxidation agent used. The much lower oxygen content detected by TGA compared to XPS (while the latter however is given in at.%) can be easily explained by the limited probing depth of XPS of about 10 nm while TGA probes the whole sample. The lower oxygen content as determined from TGA reveals, that the oxygen resides at the surface. This also rationalizes why LG2N and HG3 are comparable in their mass loss, while LG2N has a much higher surface oxygen concentration: despite the smaller surface area of LG2N compared to HG3, LG2N shows a much higher density in surface oxygen functional groups, as seen by XPS.

A more detailed look at Figure 3 reveals that the mass loss not only depends on the oxidizing agent used, but also on the carbon modification. For HG3 all curves show a steady decrease in mass loss from 100 to 1000°C with a pronounced decomposition step between 200 and 400°C, indicating that these samples contain a significant amount of more easily decomposed hydroxyl and carboxyl groups, and in conjunction with the XPS shown above it seems that hydroxyl groups are dominating. On the other hand, NA and PP treated LG2N shows a different decomposition behavior and obviously is dominated by oxygen functional groups with a higher decomposition temperature. The LG2N NASA sample is an exception as it also contains a significant amount of easily decomposable groups. It is however instructive to compare these results with the amounts of surface nitrogen as detected by XPS (Tables II and III): those samples showing decomposition of oxygen functional groups at lower temperatures (all treated HG3 samples as well as LG2N_NASA) show comparably low nitrogen surface concentrations (O_{before}/N values 3.1–5), while those with oxygen functional groups with higher decomposition show higher surface N (O_{before}/N 1.8–2.5). This is clearly not related with the decomposition temperature of urea, which is as low as 132°C, but probably with the fact that the decomposition of oxygen surface groups and concomitant defect healing takes place at low temperatures, where the reactivity of the decomposition products of urea is still low. Vice versa, one may conclude that when aiming at high nitrogen surface concentration in carbons via post treatment, the prior implementation of thermally more stable oxygen functional groups may be beneficial. Additionally, the thermal stability under oxidizing conditions of all samples was investigated by TGA in O_2/Ar gas (see supporting information Figure S2), revealing a reduced stability of the nitrogen functionalized samples, while the effect of oxygen functionalization differs for both samples.

Raman spectroscopy.—Raman spectroscopy is a valuable tool to provide information about the structure and morphology of carbon materials and their defect density.[46] The various vibrational modes of a carbon Raman spectrum may be analyzed to reveal the bonding situation, number of layers in graphite or few-layered graphene and degree of crystallinity.[47] In this study the Raman spectra evaluation was restricted to the analysis of the two major bands, the so-called D-("disordered") and G-("graphitic") band, which are typically used as an indicator for the number of defects or disordered carbon compared to the amount of graphitic material. The inset in Figure 4 presents

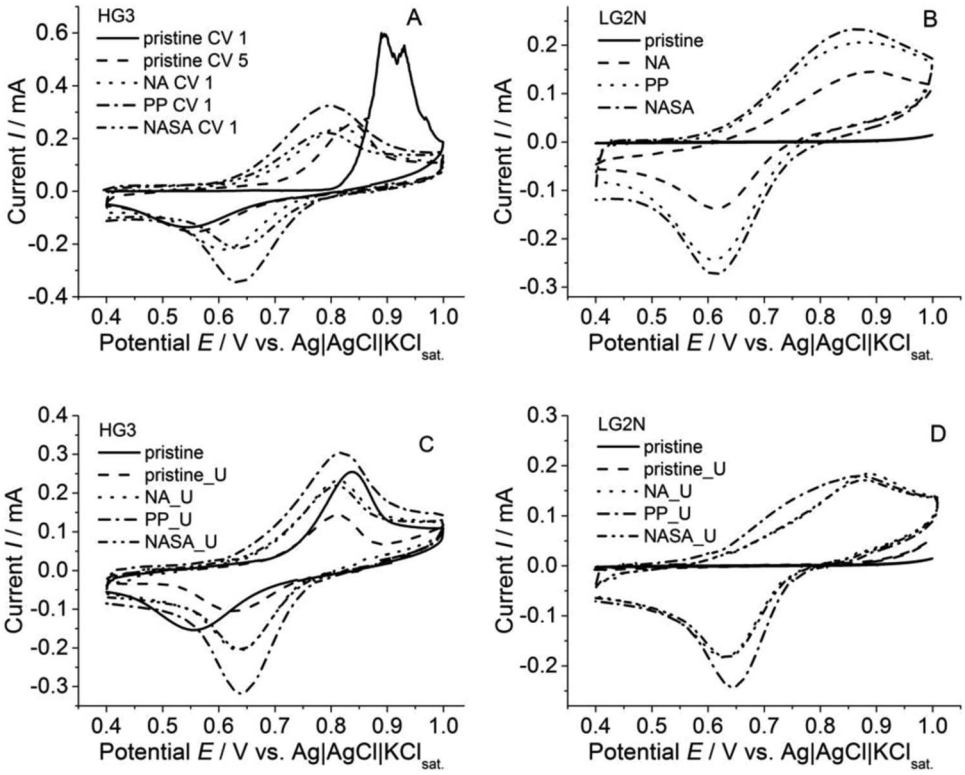

Figure 5. Cyclic voltammograms of the different Porocarb samples of this study: (a) oxidized HG3, (b) oxidized LG2N, (c) urea-treated HG3, (d) urea-treated LG2N. Recorded at RT in N_2 purged 0.01 M $VOSO_4$ in a hydrogen sulfate/sulfate buffer system at 50 mV s^{-1}.

the respective region of a Raman spectrum of HG3 showing these two bands at around 1580 cm^{-1} (G-) and 1350 cm^{-1} (D-band) as well a shoulder at 1600 cm^{-1} corresponding to the D'-band. The G-band is considerably more intense than the D-band and the spectrum resembles that of graphite[48] indicating that pristine HG3 contains mainly domains of graphitic structure. Similar spectra were obtained for the LG2N sample (not shown). Commonly, the intensity ratio between the D- and G-band (I_D/I_G) is used as a qualitative indicator of the defect density in carbon samples. Defects in the perfect graphite sheets may be introduced by the presence of structures such as five or seven-membered rings, quaternary heteroatoms or sp^3-hybridized carbon atoms. However, a separation of these individual contributions is hardly possible.

Even more, it turned out that Raman spectra recorded from different parts of the same sample were different to each other. Thus, to access the Raman-spectroscopic features of the samples as well as their variance, mapping experiments recording 250–300 single spectra were performed. A statistical evaluation allows for improved differentiation between the individual samples. For all samples, the results of the mapping experiments are given in Figure 4 in form of a Box plot providing all relevant information such as the average, the distribution, maximum and minimum of the I_D/I_G ratio. This plot allows visualizing a large amount of data and renders the required information accessible in an easy way. Both Porocarb modifications in their pristine form show a certain heterogeneity, which is enhanced or reduced depending on the treatment procedure. The data reveal differences of 0.60 between overall maximum and minimum I_D/I_G ratios which points out that single measurements are insufficient to characterize these (and probably many other) carbon samples. For comparison purpose, Vulcan XC72 as a material typically used in electrocatalysis shows a significantly narrower distribution of I_D/I_G ratios however, still this material is not completely homogeneous.

All functionalized samples show an increased average I_D/I_G ratio, ranging from 0.27 to 0.55 for HG3 and from 0.53 to 0.88 for LG2N and a maximum I_D/I_G value of 1.20 for LG2N_NASA_U is reached. Figure S3 visualizes this heterogeneity in form of false-colored maps of the I_D/I_G-ratio. Obviously, the more graphitic nature of the samples is partially but not fully destroyed during the rather harsh treatments. From TEM measurements, in particular for LG2N, one would expect a reduced I_D/I_G ratio due to removal of amorphous carbon. Keeping in mind the relatively low surface area of Porocarb, the increase in the amount of defects in the carbon structure (increased I_D/I_G ratio) is likely not only correlated to the introduction of heteroatom containing functional groups but further morphological changes must occur in the material, penetrating into the bulk. This would be also in line with the decreased thermal stability, which was observed during TGA in Ar/O_2 atmosphere (Figure S2).

As expected, the stronger oxidation agents PP and NASA lead to the highest increase in I_D/I_G ratio. On the other hand, the distribution of these values for each sample does not show such a straightforward correlation to the oxidation agent. For example PP treated HG3 shows the broadest distribution from 0.10 to 0.90 while NASA treated HG3 has a considerably narrow distribution, however, these tendencies are not found for LG2N. Keeping in mind the different morphologies of the starting materials and the different amounts of non-graphitic components, this may be explained by the different reactivity of these components toward each individual oxidation agent. Urea treatment introduces minor changes regarding the I_D/I_G ratio and distribution indicating that no significant healing of defects or introduction of new defects occurs, supporting the view that oxygen functional groups serve as reactive sites for nitrogen incorporation. A slight increase of the I_D/I_G ratio for some HG3 materials and a slight decrease for some LG2N materials should not be overinterpreted.

In the present case, Raman spectroscopy can be considered as a bulk method as the penetration and escape depths of 532 nm laser photons are between 20 and 120 nm for carbon materials.[47,49] Thus a quantitative correlation of defect density from Raman spectroscopy and surface functional groups from XPS is not straightforward. However, qualitatively one can conclude that LG2N shows both a higher defect density as well as a higher amount of surface functional groups

after oxidative treatment compared to HG3, indicating that the defect-rich material is more prone to oxidative attack.

Electrochemical characterization.—Electrochemical characterization with cyclic voltammetry was performed in order to evaluate the electrochemical performance of the materials of this study toward redox reactions of vanadium species. Typically, the peak separation between both the oxidation (VO^{2+} to VO_2^+) and reduction peak (VO_2^+ to VO^{2+}) is used as an indicator of electrocatalytic activity.[14,15,18,33,50] However, this approach was recently considered as insufficient for kinetic investigations,[35,51] in accordance with previous experience. Thus a procedure was recently established based on scanning electrochemical microscopy (SECM) which allows for a sound comparison of the redox activity of samples very different in nature (e.g. showing very different capacitive currents).[32] On the other hand, previous studies show that CV still allows for fast screening of materials and provides reliable results if samples of similar nature are compared toward the VO^{2+} to VO_2^+ redox pair, provided that a very careful electrode preparation is carried out and a statistic analysis is performed since significant scatter is observed. The evaluation of the cyclic voltammograms was restricted to a qualitative analysis only and each sample was measured 12 times to obtain reliable statistics.

The CVs of the oxidized samples of HG3 and LG2N are summarized, together with those of the pristine materials, in Figures 5a and 5b. Both pristine samples behave different. While significant anodic currents are observed during the first cycle of pristine HG3 (Figure 5a), no such currents are visible at LG2N except a slight current increase at potentials above 0.8 V, probably due to vanadyl oxidation (Figure 5b). The currents during the first scan of pristine HG3 are attributed to electrochemical carbon oxidation and their absence in LG2N is somewhat surprising since the latter sample was more prone to chemical oxidation compared to HG3. In the subsequent cycles of HG3, a constant behavior with redox peaks attributed to the VO^{2+}/VO_2^+ redox couple and a peak separation of 313 ± 32 mV is observed. All oxidized HG3 samples show well defined CVs with well pronounced redox peaks attributed to the conversion of vanadium ions throughout all five cycles. Compared to the pristine sample, a significant enhancement of the electrochemical performance is observed resulting in decreased peak separations with values of about 200 ± 30 mV. Similarly, the oxidized LG2N samples (Figure 5b) show well-defined redox peaks which are not observed in the pristine sample, however, with a slightly higher peak separation of about 290 ± 20 mV. The considerably large peak separations seem to indicate poor catalytic activity. However, note that diluted, buffered solutions compared to those of an industrial application were used. It was shown that the electrochemical activity of the positive half-cell reaction depends on the pH value as well as sulfate concentration.[52] Diluted solutions allow comparisons between CV and SECM experiments and thus with previous results.[36] Furthermore, reference tests of HG3 in concentrated $VOSO_4$ solution (not shown) revealed that the experimental scatter in this solution is much higher, impeding collection of statistical data or calculation of kinetic parameters. Consequently, to evaluate the electrocatalytic properties and to compare the individual samples on a reliable basis, diluted solutions were chosen, which also allow observing unexpected issues like the carbon oxidation during the first cycle of HG3.

The reduction peak at the LG2N samples is comparable in shape and intensity to that of HG3, however, the oxidation peak is much broader, probably indicating that more than one oxidation process is operating. Since only VO^{2+} is present as oxidable species in solution, this observation can be ascribed to the presence of two or more types of catalytic sites different in nature, with one providing a lower overpotential than the other. On the other hand, the well-defined and considerably narrow peak in the backward scan implies either only one type of catalytic sites or similar activity/overpotential of the different types. Investigations to clarify these issues are of high interest for future catalyst development and are planned for the future.

As mentioned above, due to a certain scatter in the electrochemical data a statistical analysis with twelve prepared electrodes has been conducted and the results are summarized in Table IV together with those of the nitrogen-doped samples, which will be discussed below. Obviously, NA treatment leads to a strong decrease in peak separation, while PP and NASA treatment lead to a slight further decrease. However, comparing the data from Table IV with results from XPS or Raman spectroscopy, there is no obvious correlation between peak separations and the amount or type of oxygen functional groups as well as defects in the carbon lattice. On the other hand, a certain amount of surface oxygen seems to be necessary to enhance activity of the samples.

Table IV. Peak separation between oxidation of vanadium (IV) and reduction of vanadium (V) obtained from cyclic voltammograms of Porocarb materials.

sample	Peak separation 1 ΔE/mV	Peak separation 2 ΔE/mV
HG3	313 ± 32	-
HG3_NA	220 ± 33	-
HG3_PP	187 ± 26	-
HG3_NASA	185 ± 26	-
HG3_U	184 ± 22	-
HG3_NA_U	175 ± 7	-
HG3_PP_U	182 ± 8	-
HG3_NASA_U	187 ± 13	-
LG2N	-	-
LG2N_NA	312 ± 41	-
LG2N_PP	277 ± 41	-
LG2N_NASA	283 ± 43	-
LG2N_U	-	-
LG2N_NA_U	267 ± 17	108
LG2N_PP_U	247 ± 19	135
LG2N_NASA_U	240 ± 39	88

Enhanced hydrophilicity is another effect introduced by surface oxidation. For example, for CNTs it was demonstrated that 3–5 at% surface oxygen are necessary to achieve stable suspensions in polar solvents.[53,54] In a similar experiment, 5 mg of the respective sample were added to 10 mL of distilled water and the suspensions were treated for 30 min in an ultra-sonic bath. Afterwards, a photographs of all samples was taken (supporting information, Figure S4) and the suspensions were left without agitation for 24 h. Then, photographs of all suspensions were taken again (supporting information, Figure S4). These photographs demonstrate that oxygen containing functional groups stabilize the suspension of the oxidized samples in contrast to the starting materials HG3 and LG2N, which is attributed to a stronger interaction with water and better wettability. Furthermore, SECM enabled to demonstrate for oxidized carbon nanotubes, that a certain amount of surface oxygen functional groups (min. 3 at%) increases the catalytic activity for vanadium redox reactions dramatically, likely due to improved wetting of the porous catalyst layer, while a further increase up to 8 at% did not lead to additional activity enhancement.[36] These considerations explain why functionalization is often proposed to be a required step to achieve conversion of vanadyl ions but question if selective functional groups lead to a specific catalytic enhancement.[11,12,51] Similarly, the observation in this study, that activation of Porocarb materials is largely independent of the functionalization method, supports the conclusion that wetting effects caused by functionalization are important but does not suggest a kinetic enhancement by active sites based on oxygen functional groups introduced into the carbon.

However, comparing the data for both oxidized HG3 and LG2N, it is not just the hydrophilicity, as both materials provide quite different performance with the sample having the higher surface oxygen content seems to exhibit worse electrocatalytic activity. This clearly demonstrates the dependence on the carbon modification. It has even been claimed that functionalization could lead to adverse effects, i.e. larger peak separation.[35] Thus, obviously the carbon structure and morphology has a huge influence, which is reflected in different responses

regarding wetting behavior, stability against (electro)chemical functionalization and intrinsic catalytic activity including higher electrochemically available surface. Pristine HG3 for example is less stable against electrochemical oxidation at positive potentials in comparison to pristine LG2N. On the other hand, LG2N was more easily functionalized by the used oxidation agents, resulting in almost twice the surface oxygen content.

Finally, from Figures 5a and 5b one might be tempted to use current values as an indicator of performance. However, according to previous experience already slight deviations in film quality during electrode preparations lead to significant deviations in peak currents. Thus in the present case these currents are an inadequate descriptor of performance.

Besides oxygen functionalization, nitrogen functionalization is often used to tune the electrochemical properties of carbon materials.[15,39,55] Nitrogen modifications were obtained by urea addition and heat-treatment, as described above. CVs of all samples are displayed in Figures 5c and 5d and the values of the statistical analysis are displayed in Table IV. The peak separations observed for N-modified HG3 are 180 ± 20 mV, similar to that of the oxidized samples. A nearly unchanged electrochemical behavior after nitrogen surface treatment supports the above view that wetting of the surface has a higher impact than the type of the individual functional groups, but that the general nature of the carbon material is important.

However, the more complex behavior of nitrogen-modified LG2N samples requires further attention (Figure 5d). In general, urea treated samples show a behavior similar to the oxidized ones in CV experiments including broad oxidation peaks and well-defined reduction peaks. The peak separation is once again nearly unchanged (250 ± 25 mV). A closer look reveals that in particular the oxidation peak in the CV of LG2N_PP_U has a shoulder which implies two separate peaks with the first one located at considerably low potentials (∼750 mV). On the other hand, this effect is much less pronounced in the other samples, however, still the current increase does not show the expected exponential behavior but a steady increase instead. As already discussed structure and morphology of the carbon seem to have significant influence on catalysis. As Porocarb carbons are industrial materials with a certain heterogeneity, the observed behavior may well be explained in this way.

Conclusions

The influence of O- and N-functionalization of two Porocarb modifications on their structural and electrochemical properties and in particular on their electrocatalytic activity toward vandyl ion redox reactions was studied. O-functionalization was carried out with different liquid oxidation agents (nitric acid, potassium permanganate solution, and a mixture of nitric and sulfuric acid) and the degree of functionalization as well as the kind and amount of functional groups implemented into the surface depends on both the functionalization agent as well as the carbon material, as shown by TGA and XPS measurements. However, the differences in kind and amount of functional groups are not reflected in the kinetics of vanadyl ion conversion at carbon surfaces, which leads to the conclusion that the choice of carbon material is more important than the type of modification. On the other hand, a comparison of pristine with functionalized samples underlines that in the case of Porocarb chemical activation is absolutely essential to obtain a material which catalyzes vanadium redox reactions. This activation provides a more hydrophilic surface, facilitating diffusion and adsorption of vanadyl ions. This view is corroborated by the fact, that nitrogen incorporation has equally a beneficial effect on catalytic activity, which however again does not depend on the kind of nitrogen surface functional groups. Nitrogen modification has been carried out by high-temperature urea treatment of the oxygen-functionalized samples, and a correlation between thermally more stable surface oxygen functional groups and the amount of embedded nitrogen was found.

To shed more light onto the influence of carbon structure and properties on its electrocatalytic behavior, future activities will include in situ-spectroscopic investigations using e.g. Raman and IR spectroscopy to unravel the reaction mechanism in dependence of the carbon structural features. On the other hand, from a practical point of view the performance of modified carbon materials including their long-term stability under technical conditions, i.e. in a working RFB, should be investigated.

Acknowledgments

Financial support of this project by the German ministry of education and research (BMBF) under contract 03EK3011D is gratefully acknowledged. We thank Heraeus Quarzglas GmbH & CO. KG, and in particular Dr. Dominik Samuelis, Dr. Matthias Otter and Dr. Christian Neumann for fruitful discussion throughout this project. Annett Quetschke from our institute is acknowledged for TEM and TGA measurements. Eik Koslowski from our institute is acknowledged for XPS measurements.

ORCID

Michael Bron https://orcid.org/0000-0002-3965-5691

References

1. E. Sum, M. Rychcik, and M. Skyllas-Kazacos, *J. Power Sources*, **16**(2), 85 (1985).
2. E. Sum and M. Skyllas-Kazacos, *J. Power Sources*, **15**(2–3), 179 (1985).
3. M. Skyllas-Kazacos, *J. Electrochem. Soc.*, **133**(5), 1057 (1986).
4. M. Skyllas-Kazacos, *J. Electrochem. Soc.*, **134**(12), 2950 (1987).
5. M. Rychcik and M. Skyllas-Kazacos, *J. Power Sources*, **22**(1), 59 (1988).
6. M. Skyllas-Kazacos, M. H. Chakrabarti, S. A. Hajimolana, F. S. Mjalli, and M. Saleem, *J. Electrochem. Soc.*, **158**(8), R55 (2011).
7. S. L. Mallinson, J. R. Varcoe, and R. C. Slade, *Electrochim. Acta*, **140**, 145 (2014).
8. G. Kear, A. A. Shah, and F. C. Walsh, *Int. J. Energy Res.*, **36**(11), 1105 (2012).
9. M. Ulaganathan, V. Aravindan, Q. Yan, S. Madhavi, M. Skyllas-Kazacos, and T. M. Lim, *Adv. Mater. Interfaces*, **3**(1), n/a (2016).
10. A. M. Pezeshki, J. T. Clement, G. M. Veith, T. A. Zawodzinski, and M. M. Mench, *J. Power Sources*, **294**, 333 (2015).
11. B. Sun and M. Skyllas-Kazacos, *Electrochim. Acta*, **37**(7), 1253 (1992).
12. B. Sun and M. Skyllas-Kazacos, *Electrochim. Acta*, **37**(13), 2459 (1992).
13. M. H. Chakrabarti, N. P. Brandon, S. A. Hajimolana, F. Tariq, V. Yufit, M. A. Hashim, M. A. Hussain, C. Low, and P. V. Aravind, *J. Power Sources*, **253**, 150 (2014).
14. H. Q. Zhu, Y. M. Zhang, L. Yue, W. S. Li, G. L. Li, D. Shu, and H. Y. Chen, *J. Power Sources*, **184**(2), 637 (2008).
15. Y. Shao, X. Wang, M. Engelhard, C. Wang, S. Dai, J. Liu, Z. Yang, and Y. Lin, *J. Power Sources*, **195**(13), 4375 (2010).
16. L. Yue, W. Li, F. Sun, L. Zhao, and L. Xing, *Carbon*, **48**(11), 3079 (2010).
17. Pengxiang Hou, Chang Liu, Yu Tong, Shitao Xu, Min Liu, and Huiming Cheng.
18. W. Li, J. Liu, and C. Yan, *Carbon*, **49**(11), 3463 (2011).
19. A. Parasuraman, T. M. Lim, C. Menictas, and M. Skyllas-Kazacos, *Electrochim. Acta*, **101**, 27 (2013).
20. A. Z. Weber, M. M. Mench, J. P. Meyers, P. N. Ross, J. T. Gostick, and Q. Liu, *J. Appl. Electrochem.*, **41**(10), 1137 (2011).
21. S. Zhong, M. Kazacos, R. P. Burford, and M. Skyllas-Kazacos, *J. Power Sources*, **36**(1), 29 (1991).
22. M. Gattrell, J. Qian, C. Stewart, P. Graham, and B. MacDougall, *Electrochim. Acta*, **51**(3), 395 (2005).
23. M. Graczyk-Zajac, M. Wimmer, C. Neumann, and R. Riedel, *J. Solid State Electrochem*, **19**(9), 2763 (2015).
24. B. Jache, C. Neumann, J. Becker, B. M. Smarsly, and P. Adelhelm, *J. Mater. Chem.*, **22**(21), 10787 (2012).
25. T. Wu, K. Huang, S. Liu, S. Zhuang, D. Fang, S. Li, D. Lu, and A. Su, *J. Solid State Electrochem.*, **16**(2), 579 (2012).
26. G. Wei, W. Su, Z. Wei, M. Jing, X. Fan, J. Liu, and C. Yan, *Electrochim. Acta*, **199**, 147 (2016).
27. A. J. Bard, *Electroanalytical chemistry: A series of advances*, New York, M. Dekker (1991).
28. S. Kundu, Y. Wang, W. Xia, and M. Muhler, *J. Phys. Chem. C*, **112**(43), 16869 (2008).
29. K. Balasubramanian and M. Burghard, *Small*, **1**(2), 180 (2005).
30. H. P. Boehm, *Carbon*, **32**(5), 759 (1994).
31. A. Hirsch, *Angew. Chem. Int. Ed.*, **41**(11), 1853 (2002).
32. M. Steimecke, S. Rümmler, and M. Bron, *Electrochim. Acta*, **163**, 1 (2015).
33. N. Pour, D. G. Kwabi, T. Carney, R. M. Darling, M. L. Perry, and Y. Shao-Horn, *J. Phys. Chem. C*, **119**(10), 5311 (2015).
34. C. Flox, J. Rubio-García, M. Skoumal, T. Andreu, and J. R. Morante, *Carbon*, **60**, 280 (2013).
35. J. Friedl, C. M. Bauer, A. Rinaldi, and U. Stimming, *Carbon*, **63**, 228 (2013).
36. M. Steimecke, S. Rümmler, N. Schuhmacher, T. Lindenberg, M. Hartmann, and M. Bron, *Electroanalysis*, **29**, 1056 (2017).
37. M. Park, J. Ryu, Y. Kim, and J. Cho, *Energy Environ. Sci.*, **7**(11), 3727 (2014).

38. L. Shi, S. Liu, Z. He, and J. Shen, *Electrochim. Acta*, **138**, 93 (2014).
39. S. Wang, X. Zhao, T. Cochell, and A. Manthiram, *J. Phys. Chem. Lett.*, **3**(16), 2164 (2012).
40. A. Bourke, M. A. Miller, R. P. Lynch, X. Gao, J. Landon, J. S. Wainright, R. F. Savinell, and D. N. Buckley, *J. Electrochem. Soc.*, **163**(1), A5097 (2015).
41. L. Cao, M. Skyllas-Kazacos, and D.-W. Wang, *J. Electrochem. Soc.*, **163**(7), A1164 (2016).
42. M. Skyllas-Kazacos and M. Kazacos, *J. Power Sources*, **196**(20), 8822 (2011).
43. J. L. Hueso, J. P. Espinós, A. Caballero, J. Cotrino, and A. R. González-Elipe, *Carbon*, **45**(1), 89 (2007).
44. T. Ramanathan, F. T. Fisher, R. S. Ruoff, and L. C. Brinson, *Chem. Mater.*, **17**(6), 1290 (2005).
45. V. Datsyuk, M. Kalyva, K. Papagelis, J. Parthenios, D. Tasis, A. Siokou, I. Kallitsis, and C. Galiotis, *Carbon*, **46**(6), 833 (2008).
46. A. C. Ferrari and J. Robertson, *Phys. Rev. B*, **61**(20), 14095 (2000).
47. R. L. McCreery, *Chem. Rev.*, **108**(7), 2646 (2008).
48. F. Tuinstra, *J. Chem. Phys.*, **53**(3), 1126 (1970).
49. Z. Marković, D. Kepić, I. Holclajtner Antunović, M. Nikolić, M. Dramićanin, M. Marinović Cincović, and B. Todorović Marković, *J. Raman Spectrosc.*, **43**(10), 1413 (2012).
50. J. Melke, P. Jakes, J. Langner, L. Riekehr, U. Kunz, Z. Zhao-Karger, A. Nefedov, H. Sezen, C. Wöll, H. Ehrenberg, and C. Roth, *Carbon*, **78**, 220 (2014).
51. M.-A. Goulet, M. Skyllas-Kazacos, and E. Kjeang, *Carbon*, **101**, 390 (2016).
52. G. Oriji, Y. Katayama, and T. Miura, *Electrochim. Acta*, **49**(19), 3091 (2004).
53. T. J. Aitchison, M. Ginic-Markovic, J. G. Matisons, G. P. Simon, and P. M. Fredericks, *J. Phys. Chem. C*, **111**(6), 2440 (2007).
54. J. M. González-Domínguez, M. González, A. Ansón-Casaos, A. M. Díez-Pascual, M. A. Gómez, and M. T. Martínez, *J. Phys. Chem. C*, **115**(15), 7238 (2011).
55. Y. Shao, J. Sui, G. Yin, and Y. Gao, *Appl. Catal. B: Environmental*, **79**(1), 89 (2008).